2014-08

The dispersal of phytoplankton populations by enhanced turbulent mixing in a shallow coastal sea

Cross, J

10.1016/j.jmarsys.2014.03.009
Journal of Marine Systems
Elsevier BV

The dispersal of phytoplankton populations by enhanced turbulent mixing in a shallow coastal sea

Jaimie Cross[a,*], W. Alex M. Nimmo-Smith[a], Philip J. Hosegood[a], Ricardo Torres[b]

[a] *School of Marine Science and Engineering, Plymouth University, Drake Circus, Plymouth PL4 8AA, UK*
[b] *Plymouth Marine Laboratory, Prospect Place, The Hoe, Plymouth PL1 3DH, UK*

Abstract

A single tidal cycle survey in a Lagrangian reference frame was conducted in autumn 2010 to evaluate the impact of short-term, episodic and enhanced turbulent mixing on large chain-forming phytoplankton. Observations of turbulence using a free-falling microstructure profiler were undertaken, along with near-simultaneous profiles with an in-line digital holographic camera at station L4 ($50^{\circ}\,15'$ N $4^{\circ}\,13'$ W, depth 50 m) in the Western English Channel. Profiles from each instrument were collected hourly whilst following a drogued drifter. Results from an ADCP attached to the drifter showed pronounced vertical shear, indicating that the water column structure consisted of two layers, restricting interpretation of the Lagrangian experiment to the upper ~ 25 m. Atmospheric conditions deteriorated during the mid-point of the survey, resulting in values of turbulent dissipation reaching a maximum of $10^{-4}\,\mathrm{W\,kg^{-1}}$ toward the surface in the upper 10 m. Chain-forming phytoplankton $> 200\,\mu$m were counted using the data from the holographic camera for the two periods, before and after the enhanced mixing event. As mixing increased phytoplankton underwent chain breakage, were dispersed

*Corresponding author. 3a Reynolds Building, Drake Circus, Plymouth University, Plymouth PL4 8AA UK
Email address: jaimie.cross@plymouth.ac.uk (Jaimie Cross)

by advection through their removal from the upper to lower layer and subjected to aggregation with other suspended material. Depth averaged counts of phytoplankton were reduced from a maximum of around 2050 L^{-1} before the increased turbulence, to 1070 L^{-1} after, with each of these mechanisms contributing to this reduction. These results demonstrate the sensitivity of phytoplantkon populations to moderate increases in turbulent activity, yielding consequences for accurate forecasting of the role played by phytoplankton in climate studies and also for the ecosystem in general in their role as primary producers.

Keywords: Turbulence; L4; Phytoplankton dispersal; Holographic imaging; Flocculation

1. Introduction

Turbulence, be it generated at the surface or by internal processes, may have a controlling influence on the movement and distribution of phytoplankton, acting to keep non-motile phytoplankton in suspension (Jumars et al., 2009). This is particularly relevant in shallow coastal seas, where the majority of energy associated with tidal activity is dissipated. Turbulence can also act against stratification to mix nutrients across density gradients, so turbulent patches within the thermocline may impact on bloom dynamics by acting as sites of enhanced primary productivity (Sharples et al., 2001; Steinbuck et al., 2009).

Investigating the impact that turbulence has on individual populations of phytoplankton is not straightforward, and would typically be conducted in laboratory microcosms. Within these idealised environments our understanding of the response of phytoplankton to turbulence has been advanced considerably, including examining the influence upon nutrient uptake (Romero et al., 2012), communtiy composition and size (Arin et al., 2002), and the influence of varying levels of turbulence itself (Cozar and Echevarria, 2005). Similar investigations in the field are uncommon, typically due to the limi-

tation of an uncontrolled environment or the absence of appropriate instrumentation to tackle the problem. Often, destructive techniques are used to sample the water column, which can readily damage phytoplankton giving misleading information on biomass or size (Gallienne and Robins, 2001). Non-destructive methods such as laser transmissometry are beginning to prove popular (Rzadkowolski and Thornton, 2012), although it is unclear how well the statistics gained from these instruments translate to the characteristic size and shape of phytoplankton in the marine environment.

Image analysis has been shown to be a useful non-destructive method for analysing phytoplankton *in situ* (Zarauz et al., 2009; Stemmann and Boss, 2012). Methods such as digital photography allow some indication of the organisms under study, though the resulting image resolution may be considered impractical for a more comprehensive analysis of particle type. The emerging technology of holographic imaging offers detailed images of suspended particles under a range of conditions, generating particle statistics such as size and number density without the need to disturb particles from their natural environment (Graham and Nimmo Smith, 2010; Graham et al., 2012). The work presented here utilises holographic imaging for all observations of phytoplankton.

The aim of this paper is to investigate the response of a phytoplankton community to short-term, enhanced turbulent mixing at station L4 in the Western English Channel. L4 may be regarded as typical of the shallow shelf system of the United Kingdom. Whilst exhibiting seasonal stratification, this site is prone to frequent bouts of increased mixing from inclement weather systems (Groom et al., 2009). As such, L4 is well suited to providing an insight into phytoplankton dynamics when exposed to differing types of physical forcing.

2. Methods

2.1. Survey location

Station L4 resides approximately 10 km south of Plymouth at 50° 15′ N 4° 13′ W where the water depth is around 50 m with a seabed predominantly consisting of sand (Figure 1). Long-term data exist for temperature and salinity at L4, along with a wealth of information on phytoplankton and zooplankton. With the proximity to the coast, and also to the outflow of freshwater from the local rivers, the L4 site forms a central part of the Western Channel Observatory (WCO). The long-term data indicates that the site is well-mixed during the winter, before the onset of thermal stratification in spring that is maintained through to the autumn months. The stratified water column has an average difference in temperature of 2 °C between the upper and lower layers (Fishwick, 2008). The site is characterised by a dominant semi-diurnal tide, experiencing a maximum range of over 5 m that generates currents of 0.5-0.6 m s^{-1} at the surface.

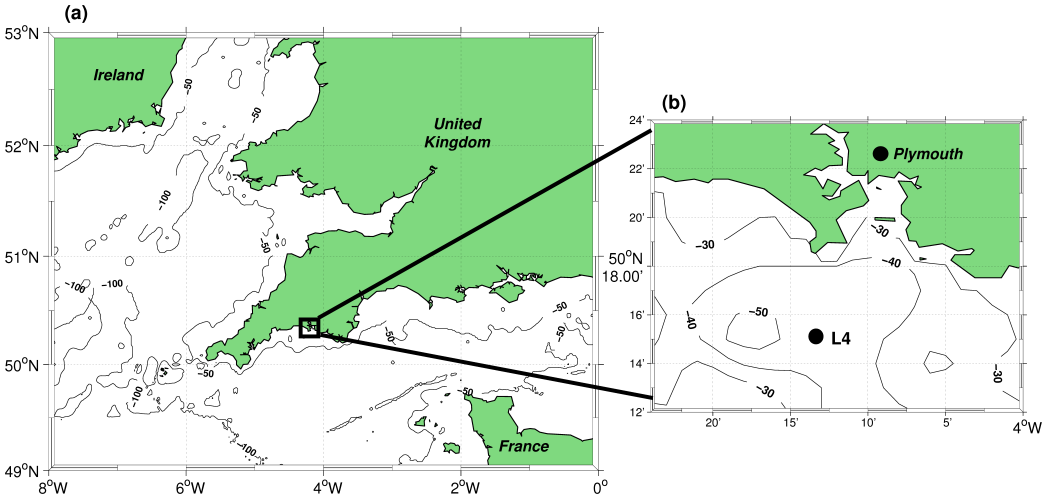

Figure 1: Map of the southern part of the United Kingdom (a) with exploded section noting the location of Station L4, approximately 10 km south of Plymouth (b)

2.2. Physical measurements

Measurements utilising an array of instruments were undertaken on the 22nd September 2010 aboard the *RV Plymouth Quest*, during spring tides. The experiment formed part of a set of surveys detailed in Cross et al. (2013), though much of the method is reproduced here for clarity. All instruments were deployed in a Lagrangian reference frame whilst following a drifter drogued by a holey sock positioned at 3-12 m. Within the drifter-drogue assembly, a 600 kHz Acoustic Doppler Current Profiler (ADCP) was fixed within a neutrally-buoyant submersible at an approximate depth of 20 m. The ADCP sampled at 2 s intervals with a bin size of 0.5 m, with the depth of the first good bin at 21 m. The device was fixed in a downward-looking position and was able to resolve the level of current shear present for the lower part of the water column. The vessel relocated to the drifter each hour, and measurements were obtained whilst the drifter was no further than 100 m from the ship. A free-fall microstructure profiler, the ISW Wassermesstechnik MSS-90, was utilised to observe the turbulent velocity shear. The number of profiles taken during each hour ranged from 6-8. The MSS-90 contains a number of sensors including optical backscatter (OBS), a fluorometer and conductivity, temperature and depth (CTD) probe. The dissipation rate of turbulent kinetic energy was estimated from the small-scale shear and assuming isotropy is defined as:

$$\varepsilon = 7.5\nu\langle(\partial u/\partial z)^2\rangle, \tag{1}$$

where ν is the kinematic viscosity, which in seawater takes the value of about $10^{-6}\,\mathrm{m^2\,s^{-1}}$, and $\partial u/\partial z$ represents the spatial derivative of the horizontal current component, u, in the vertical direction, z. The angled brackets denote a suitable time average, and the units of turbulent dissipation are given in $\mathrm{W\,kg^{-1}}$. MSS-90 profiles begin at a depth of 5 m, due to the potential for contamination from the motion of the boat induced by wave activity (Lozovatsky et al., 2006). The MSS-90 samples at a rate of 1024 Hz with a typical fall

speed of $0.5\,\mathrm{m\,s^{-1}}$. Such high frequency measurements allow for great confidence in the estimate of ε. Common to the use of these instruments, the error associated with each measurement is around $\pm 50\%$ (Simpson et al., 1996; Rippeth and Inall, 2002). It should be noted that with moderate turbulence generating values for ε of around $10^{-6}\,\mathrm{W\,kg^{-1}}$, such as would be observed at L4, it is readily shown that the uncertainty with each measurement is low (e.g. Prandke 2005).

2.3. Holographic camera

An in-line digital holographic imaging system, the holocam, was also deployed. The holocam is mounted on a steel frame along with a CTD, and is described fully in Graham and Nimmo Smith (2010). Briefly, the system contains a laser light source that illuminates a sample volume containing phytoplankton particles which scatter the light, whereupon an interference pattern is generated and subsequently recorded by a charge-coupled device (CCD). The resulting hologram is then computationally reconstructed post-deployment to give in-focus images of every particle in the sample volume, allowing for the calculation of particle statistics such as volume concentration and size distribution. Each raw hologram has a pixel resolution of $4.4\,\mu\mathrm{m}$, and is 1536 x 1024 pixels in size, yielding a sample volume of $1.65\,\mathrm{cm^3}$ which is later scaled up to one litre during post-processing. In practical terms the minimum particle size resolved by this system is around $25\,\mu\mathrm{m}$, with the maximum size limited only by the size of the CCD, here in excess of 6 mm. The holocam was profiled vertically through the water column once each hour, near-simultaneously with the MSS profiles. The sampling frequency was 5 Hz with a profiling speed typically in the range of 0.2-0.4 $\mathrm{m\,s^{-1}}$, thus samples were obtained at a vertical resolution of around 5-6 cm.

The average number of holograms taken during a given profile of the instrument is around 1000; however the number of images for a given section of the water column may vary with the minor variation in fall speed range or water column properties. With the sample volume of each image, the

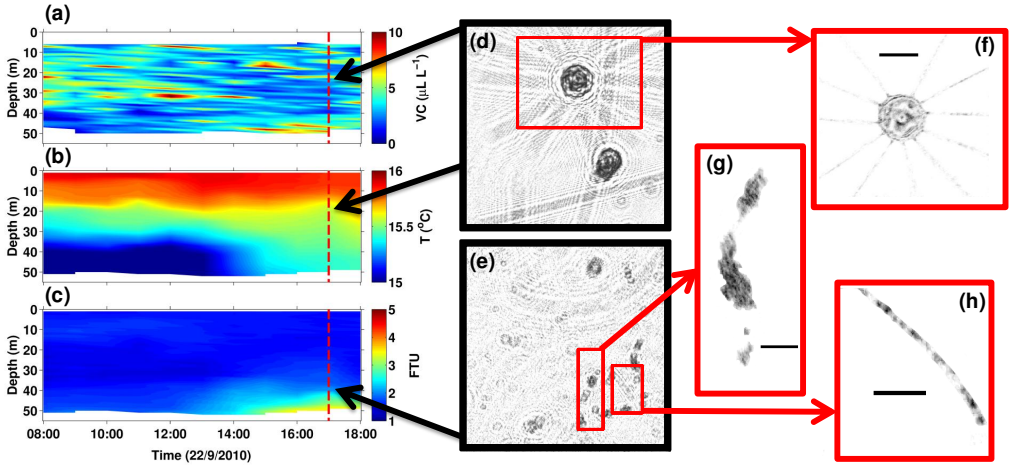

Figure 2: Illustration of the initial particle analysis using signals of interest from the MSS. Part (a) shows the total particle volume concentration (holocam), (b) and (c) the response from the temperature and OBS sensors (MSS). Parts (d) to (h) represent a step-wise view of selecting raw holograms prior to numerical reconstruction in order to establish the type of particle present. The scale bar in (f) is 200 μm, in (g) and (h) 100 μm. The dashed vertical line on plots (a), (b) and (c) represents the time of high water.

total volume of water sampled during each profile would be in the region of 1.5-2 L. An illustration of how the holocam is used to assess the particle environment is further displayed in Figure 2. The first step of this analysis is to locate the raw holograms that relate to the area of the water column that is of interest. Regions of interest (ROI) may be defined within each hologram and numerically reconstructed, revealing a sharp and in-focus image of each particle (Figure 2f to h).

An additional technique was employed to determine how phytoplankton may be altered by changes to their physical environment, and also where within a tidal cycle their number is shown to vary. Prior to this work, such enumeration of phytoplankton has not been possible *in situ*. Within the size range of phytoplankton that the holocam may reliably resolve, phytoplankton biomass at L4 is dominated by chain-forming phytoplankton (Widdicombe et al., 2010), whereby within each image a colony of multiple diatom cells is regarded a single suspended particle. Diatom chains are routinely found to grow to several mm in size and are readily identifiable from the image data. However, to maximise efficiency when counting individual colonies, only phytoplankton $\geq 200\,\mu$m were identified and recorded. The assumption is made that this threshold would be sufficient to identify changes to the phytoplankton population brought about by enhanced turbulence.

A simple, graphical user interface was designed in Matlab which took both a flattened, reconstructed image of a 1024×1024 ROI in addition to the same raw, unreconstructed hologram as inputs. Blocks of images were collated within 5 m intervals. Phytoplankton were first identified as present through simple observation of each image. Upon identification, selection of the phytoplankton was achieved through the click of a computer mouse. The interface stored each click as a single phytoplankter, allowing for the calculation of the mean number of phytoplankton per unit volume of one litre. Throughout this paper, the term number is used to refer to this metric when describing changes to the phytoplankton population.

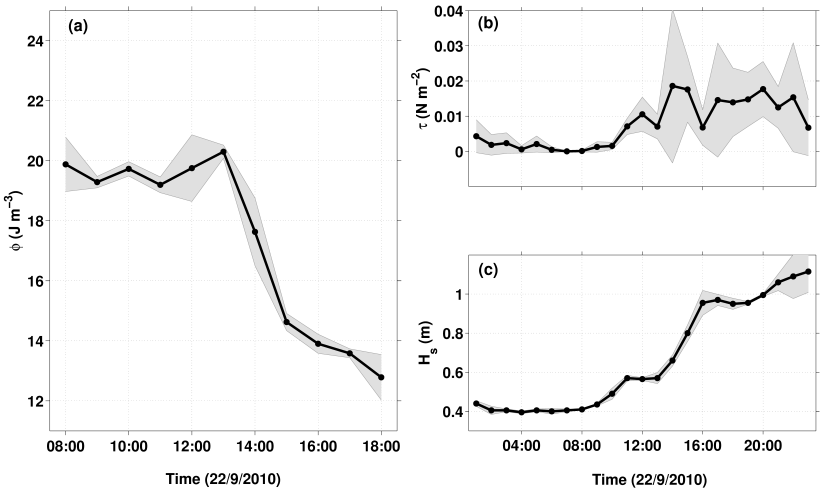

Figure 3: The rapid change in water column energetics brought about by the inclement conditions. In (a), the potential energy anomaly (PEA), ϕ, (b) local wind stress, τ and (c) significant wave height, H_s, from a nearby wave buoy in Looe Bay.

3. Results

The duration of the survey was for only 11 hours, as the sampling activity was affected by instrument failure brought about by inclement conditions. Throughout the survey the weather conditions deteriorated which resulted in enhanced mixing from the surface, partially eroding the stratification present. However, these conditions resulted from a relatively moderate increase in wind stress, with values at its peak of $1.9\,\mathrm{x}\,10^{-2}\,\mathrm{N\,m^{-2}}$(Figure 3b).

Wave conditions were assessed by utilising data from the Looe wave buoy, located at 50.34° N 04.41° W, which is 17 km from L4. The buoy is situated in water with a depth of around 12 m. The average wind direction throughout the period where wind stress increases was from the south at 180°. The buoy records a value for H_s, the significant wave height, which is taken to be the average wave height of one-third of the highest waves. Coincident with the increase in τ is a corresponding increase in H_s. Whilst the corresponding wave energy generated by each site would differ markedly due to the shallow

depth of the Looe Bay buoy, it is nonetheless indicative of the impact the increased wind activity has on the region.

The potential energy anomaly, (PEA), describes the amount of energy required to bring about a completely mixed water column. Simpson et al. (1990) described the PEA, in units of $\mathrm{J\,m^{-3}}$, as follows:

$$\phi = \frac{1}{H}\int_{-H}^{0}(\bar{\rho}-\rho)\,gz\mathrm{d}z \tag{2}$$

here, H is the water depth, ρ density, g acceleration due to gravity with the overbar defining a depth-average. The evolution of ϕ displays the rapid alteration to the structure of the water column (Figure 3a). For the initial six hours of the survey values of ϕ range between 19.2-20.3 $\mathrm{J\,m^{-3}}$ before the marked reduction, to a minimum of 12.8 $\mathrm{J\,m^{-3}}$ at hour 11. However, when observing the results from the ADCP, it is not thought that the coincident wind and wave activity is entirely responsible for this rapid change (Figure 4). Due to the position of the ADCP, velocity is available for the lower part of the water column only. The presence of vertical shear is marked, and suggests that there is the potential for the composition of the observed water mass to be readily altered by processes other than vertical mixing. This notion is confirmed by the Progressive Vector Diagram (PVD) which suggests the maximum separation between the middle of the water column and the bottom to be of the order of $\sim$1 km (Figure 5). A comparative analysis for the upper layer was not possible due to unreliable GPS data from the drifter.

The maximum value of velocity magnitude, U, in the lower part of the water column is 0.39 $\mathrm{m\,s^{-1}}$ at the around midday, shortly before the start of the increased wind and wave activity. In the latter part of the survey, U was reduced with values close to 0.2 $\mathrm{m\,s^{-1}}$. The reduced tidal velocity has resulted in lower values of ε, with the maximum dissipation of 10^{-5} $\mathrm{W\,kg^{-1}}$ here not extending above 40 m (Figure 4c). Of particular note was the increased ε

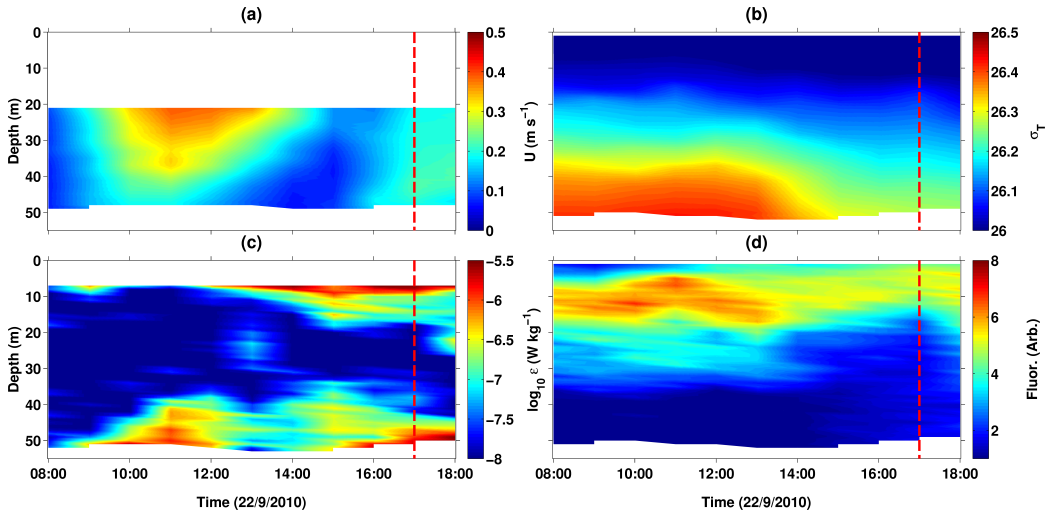

Figure 4: Water column structure and properties. Plot (a) gives velocity magnitude, U, provided by the ADCP on the drifting float for the lower part of the water column, plot (b) density, σ_T, (c) turbulent dissipation, ε, and plot (d) fluorescence in arbitrary units. Plots (b), (c) and (d) are from the MSS observations. The dashed vertical line represents the time of high water.

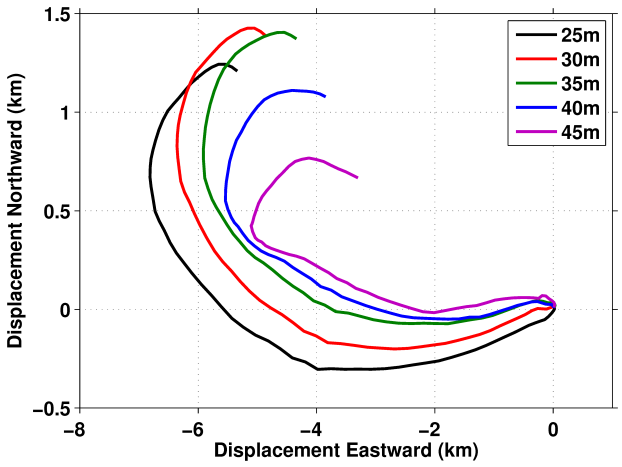

Figure 5: Progressive Vector Diagram for the lower part of the water column covered by the downward-facing ADCP.

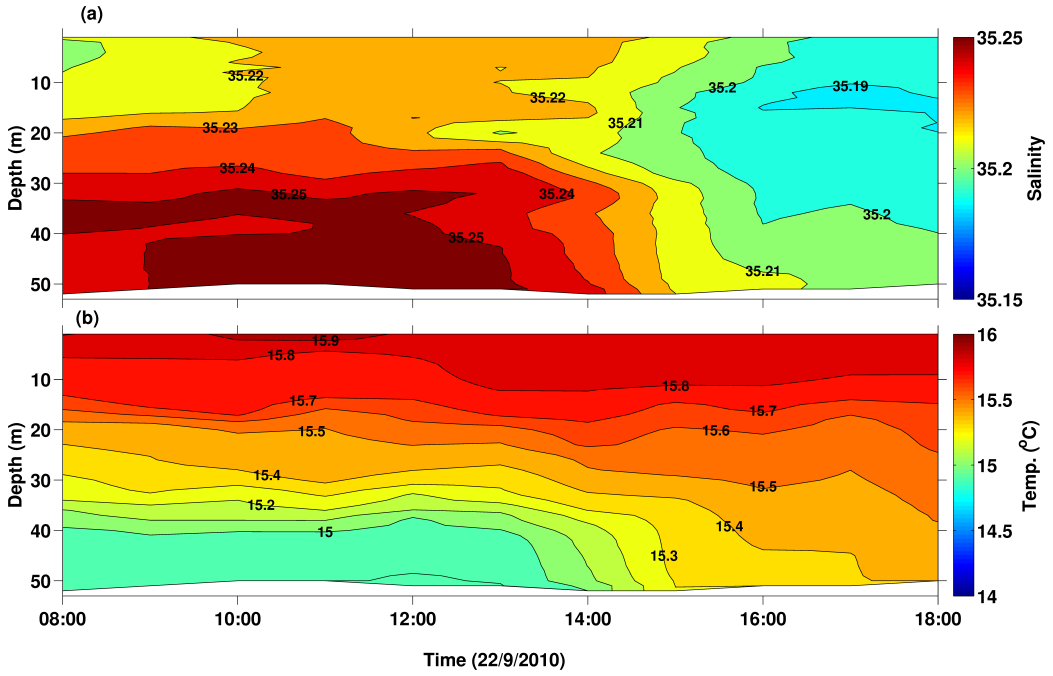

Figure 6: Contoured plots of salinity (a), and temperature (b) for the entire survey.

in the upper part of the water column toward the end of the survey. This is likely a result of the increased wind and wave energy, where dissipation rates of around 10^{-4} W kg^{-1} were observed at a depth of 6-7 m. Increased mixing from turbulence continued with depth, albeit to a lesser extent, with values of ε approaching 10^{-6} W kg^{-1}, similar to that brought about by tidal forcing earlier in the survey. However, this enhanced mixing is not observed to extend to depths below 30 m at any point.

Further evaluation of the underlying processes that influence water column density was undertaken through the analysis of temperature and salinity (Figure 6). The influence of both vertical mixing and advection can be seen at the two points of interest in the survey. Although exaggerated by scale, the water column freshens slightly toward the latter part of the survey, with values for S in the upper layer being reduced by around 0.03. This small change is unlikely to be the result of vertical mixing, it is more likely the

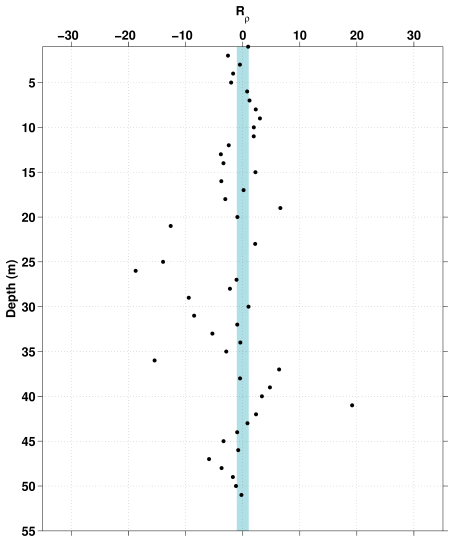

Figure 7: Density ratio for the 16.00 period, the period where vertical mixing in the upper layer is shown to occur. The shaded blue region denotes the -1 to 1 range. Values that fall within this range indicate that density is more strongly influence by salinity, and *vice versa*.

result of the interspersing of filaments of fresher water with the Lagrangian water mass. Filaments such as these are likely to be encountered at this site due to the input from the nearby riverine sources (Smyth et al., 2010). There is some indication that the increased input of energy into the upper layer is beginning to homogenise temperature. Maximum surface temperatures at 10.00 are shown to be 15.9^{o}C. This is reduced at the 16.00 point by 0.1^{o}C to 15.8^{o}C, and the depth at which this value is observed decreases from around 5 m to 10 m. To establish the relative influence of both temperature and salinity on the density of the water column, the density ratio, given as:

$$R_\rho = \frac{\alpha(\Delta T)}{\beta(\Delta S)}, \tag{3}$$

(where $\alpha = \frac{1}{\rho_0}\frac{\partial \rho}{\partial T}$ is the thermal expansion coefficient and $\beta = \frac{1}{\rho_0}\frac{\partial \rho}{\partial S}$ the haline contraction coefficient) was calculated for the point of the survey where vertical mixing begins to homogenise temperature (Figure 7). The water

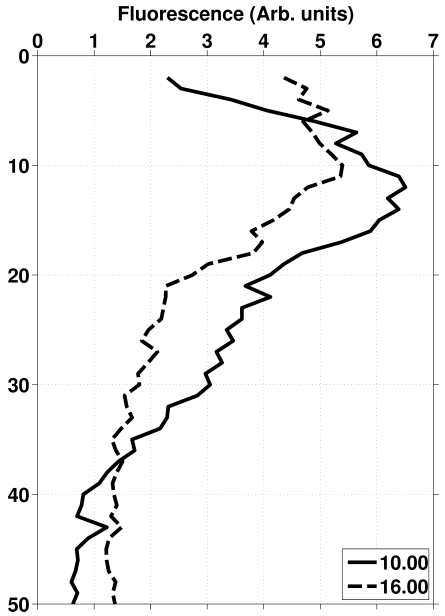

Figure 8: Profiles of Fluorescence (in arbitrary units) for the two selected time periods of prior to the increase in atmospheric forcing and after.

column will be most strongly influenced by salinity if the values of R_ρ fall within the -1 to 1 range. Whlist salinity is shown to exert some influence over density for this period, overwhelmingly it is shown to be temperature that dominates. This is particularly apparent in the upper 25 m of the water column, where all but five of the points lie outside of the -1 to 1 range.

This analysis is driven by focusing on the signals of interest provided by the MSS. Fluorescence responds to the increase in mixing by reducing strength in the latter part of the survey (Figure 4d). Looking in more detail at the two periods of interest, a quantifiable difference in fluorescence is observed (Figure 8). Integrating both periods with respect to depth shows that the latter period returns a signal that is reduced by around 15%, as the particles that contribute to the total begin to be affected by the conditions. Using the technique of counting the population of large phytoplankton particles, it was possible to see if this change was reflected in the number identified. For the earlier period, the number of phytoplankton is markedly above that

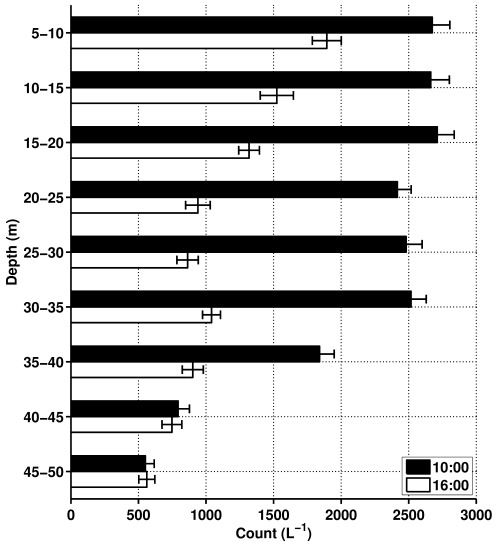

Figure 9: Phytoplankton counts before and during the enhanced period of surface mixing. The two selected time periods are as illustrated.

which is observed in the later part of the survey. Many of the depth intervals above 35-40 m contain counts of phytoplankton above 2500 L^{-1}, corresponding to the large patch of fluorescence. The later period, shown as the white bars of Figure 9, broadly follows the same pattern in that the largest values are observed closer to the surface before reducing markedly with increasing depth. Only the uppermost two depth intervals contain values greater than 1500 L^{-1}, however, as the impact of the increased mixing begins to alter the phytoplankton population. The depth-averaged value for 16.00 is slightly more than 1000 L^{-1}, almost half of that at 10.00. Differences are also observed in the particle size distribution (PSD), where for the earlier period the holocam measures a greater number of large particles and fewer smaller particles (Figure 10). This situation is reversed for the later period.

These differences appear despite the total particle volume concentration remaining similar throughout the survey. This is highlighted by Figure 2a, and shown in more detail by the depth profiles of Figure 11. This indicates

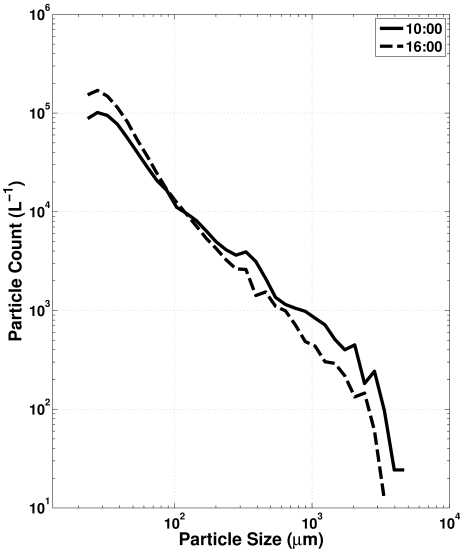

Figure 10: The particle size distributions for both 10.00 and 16.00.

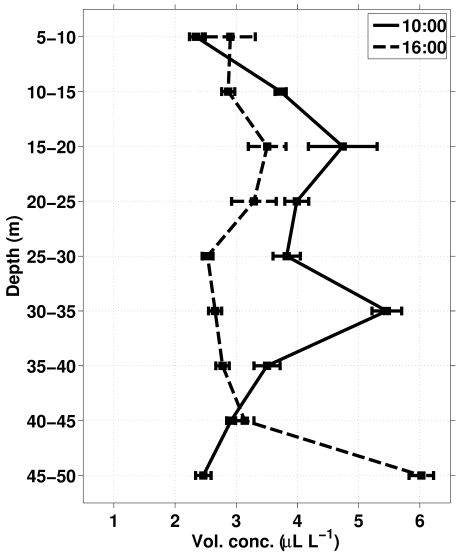

Figure 11: Total particle volume concentration from the holocam for the contrasting periods of the tidal survey, as labelled.

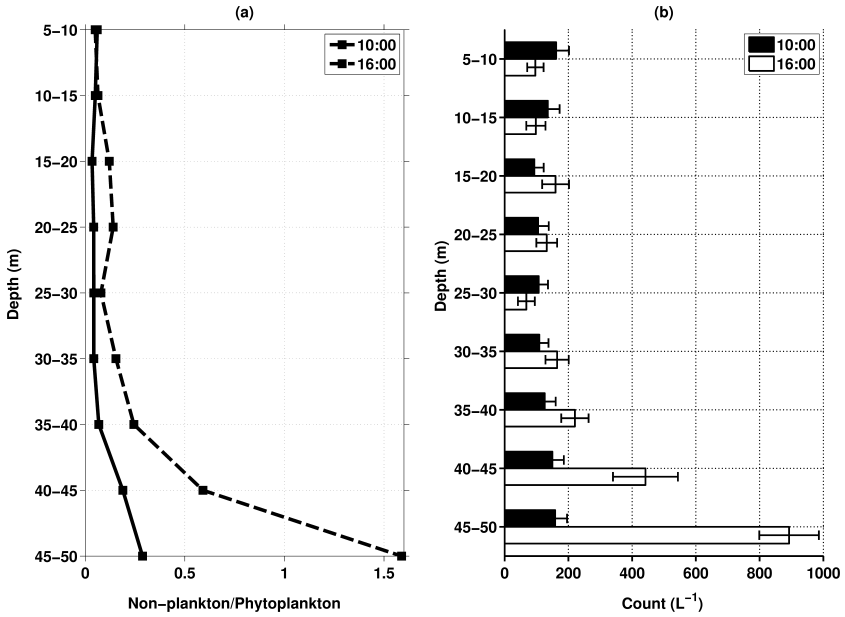

Figure 12: Plot (a) displays the ratio of the number of phytoplankton to non-planktonic particles, where values < 1 indicate a dominance of phytoplankton particles. Plot (b) gives the number of non-planktonic particles (flocs, mineral grains etc.) $> 200\,\mu$m.

that, as broadly the same amount of material is present both before and after the increase in atmospheric forcing, an explanation for the marked difference between the counts of phytoplankton is required. The PSD is suggesting that a greater number of smaller particles exist at 16.00, indicating that the large diatoms that dominate the suspended particle population of L4 are possibly being reduced in size by the increase in turbulence, below the threshold of manual identification.

The image analysis further allows the identification of multiple particles of various types. A separate exercise was conducted to determine the number of large particles from the non-planktonic fraction, that is those that comprise flocs, or aggregations of pieces of biological matter and mineral-type grains or clays. This enabled the calculation of the ratio of non-plankton to phytoplankton particles to be assessed (Figure 12a). In calculating this ratio, where values < 1 indicate a dominance of phytoplankton, for the later

part of the survey values of the ratio were higher suggesting the increased presence of non-plankton particles. However, it is noted that the increase is largely restricted to the lower part of the water column and most probably linked to resuspension of material from the bed (Figure 12b). In the upper part, there are only two intervals where a larger number of non-planktonic particles are observed for the 16:00 time point.

4. Discussion and Conclusions

The onset of poor weather gave an opportunity to assess the response of the phytoplankton to enhanced turbulence from the surface. The plot of fluorescence (Figure 4d) reinforces the impact of the increased mixing, and appears to have been immediately altered. Within the upper layer, commensurate with the partial erosion of the thermocline is the dispersal of the fluorescence signature which at 10:00 was at its strongest at the base of the density interface. However, the increased turbulence brought about by the atmospheric conditions does not penetrate the entire water column. Given the presence of vertical shear (Figure 4a), it is apparent that the water column could be considered as existing as two layers, with only the upper $\sim$25 m remaining part of the Lagrangian experiment. It is likely that the rapid change to the structure of the water column and subsequent alteration to the phytoplankton population has been brought about by the combined action of advection in the lower layer, and mixing from the enhanced turbulence in the upper.

That the upper layer undergoes such rapid change in response to the coincident increase in wind and wave activity has been previously reported during a recent study by Sutherland et al. (2013). Enhanced mixing was observed to erode stratification shortly after an observed increase to the wind speed, with little lag before the expected increase to the level of turbulence was recorded. A similar pattern in the temperature signal is observed here, albeit on much reduced scales. Further, whilst the salinity signal is suggestive

of advection also playing a role in the upper layer, the observed change is very small. The maximum surface to bottom salinity gradient is only 0.03 at any point in the survey. Smyth et al. (2010) suggest that filaments of fresher water can readily enter into a sampled frame of reference as a result of the proximity of L4 to riverine sources. However, when this occurs salinity values are often reduced by up to 1 in the upper 25 m, a difference of two orders of magnitude over what is observed here. As temperature is also shown to dominate at the 16.00 time point (Figure 7), it is likely the assumption that these observations are made within a single water mass for the upper layer is sound.

As with the fluorescence signal, the phytoplankton population during the earlier part of the survey is dispersed, encompassing a wider range of depth intervals and decreasing the number of large phytoplankton observed overall. Periodic erosion of the thermocline similar to that reported here has been observed across tidal cycles previously, albeit with respect to the enhanced tidally-induced turbulence displacing the thermocline upwards (Sharples, 2008). However, few if any studies have captured the partial erosion of stratification during a tidal cycle and also been able to comment on the subsequent dispersal of the resident phytoplankton in response.

The distribution of phytoplankton has been substantially altered between the two periods, so much so that the depth averaged values for the later period are almost halved. We suggest that there are three main reasons for this change. The reduction in the length of diatom chains below the identification threshold of 200 μm in response to the enhanced turbulence in the upper layer is seen to occur. Though in the absence of data quantifying the average lengths of diatom chains before and after the increased mixing, it is accepted that this interpretation may be open to question. However, the reduction displayed by the PSD for the larger particle size fraction is indicative that this is accurate (Figure 10). Further, the PSD is generated by reference to the major axis length (MAL) of a given particle. Consistently throughout

this survey, diatoms were the dominant particle present within each image. Therefore, the PSD returned by the holocam is heavily influenced by the long, chain-forming phytoplankton at sizes above the 200 μm threshold, offering additional support to the notion that chain breakage is a key mechanism for reducing the count. Whilst chain breakage might not be considered dispersal as such, to our knowledge this coincident response to turbulent mixing from a phytoplankton population has not been previously observed *in situ*.

The potential for phytoplankton to be advected away from the sampled water mass is an additional means by which the counts might be reduced. It is well accepted that there exists a negative relationship between fluorescence and increased turbulence (e.g. Mitchell et al., 2008; Prairie et al., 2011). Typically, in the presence of turbulence, phytoplankton tend to sink more rapidly, as recently demonstrated by Macias et al. (2013). If advection is playing a prominent role at this time, then systematic removal from the upper to lower layer may be occurring, with the sheared flow acting to disperse the population out of the sampled reference frame. This is potentially supported by the increase in fluorescence toward the bed at the 16:00 point (Figure 8), but also in the upper layer as presumably the higher values for fluorescence at the earlier time point need to balanced elsewhere.

There is also a contribution to the reduction in the counts resulting from turbulence aggregating the particles, altering their classification under our scheme from phytoplankton to a non-plankton particle. The advantage of using the holocam is that it allows for the *in situ* analysis of particles that other methods are unable to provide, including water sampling. If it is accurate that turbulence is increasing the potential for aggregation, then the images must contain evidence that this is happening. This is indeed the case, as is demonstrated by Figure 13, where the examples within this image are taken from both the upper and lower layers of the water column. Clearly, given the amount of material present in the lower layer, aggregation is more likely to be promoted here. This was also the case toward the bed for the earlier part

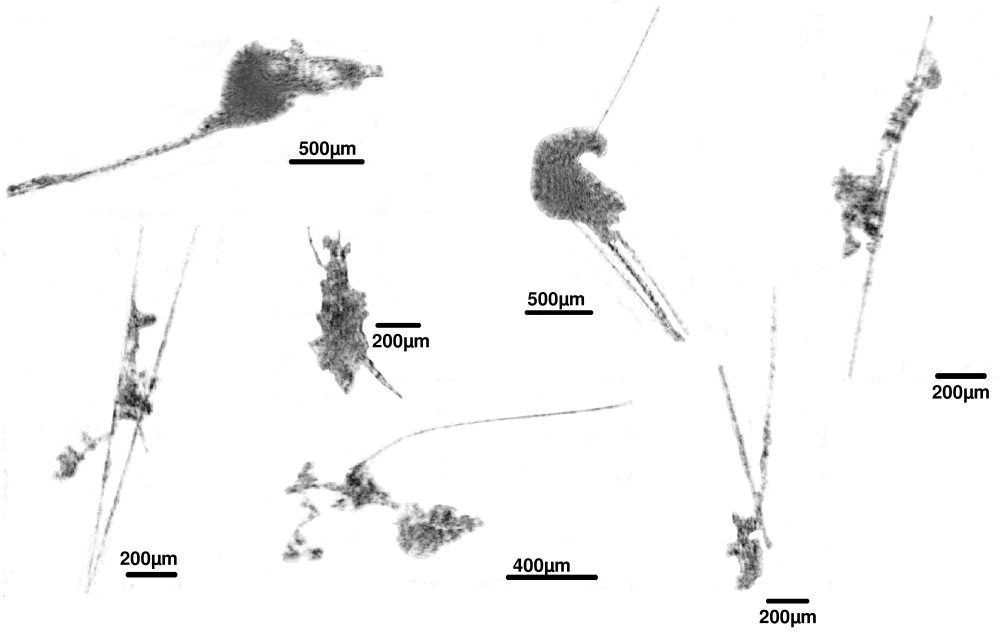

Figure 13: Montage illustrating the large number of diatom chains that have changed 'classification' from a phytoplankton to non-plankton particle under the scheme used throughout this work. The scale bars for each particle are as labelled.

of the survey where aggregation of particles similar to these examples also occurs. For all cases where aggregation is observed (i.e. toward the bed at 10:00 and in both the upper and lower layers at 16:00), it is during elevated levels of ε of around 10^{-6} W kg^{-1} and above.

The potential for turbulence to break up suspended marine particles is well understood (Hill, 1998; Manning and Dyer, 1999; Jago et al., 2006). However, it is less certain as to the strength of turbulence necessary to cause chain-forming phytoplankton to undergo breakage. The level of turbulence observed during the latter part of the survey, whilst higher in the upper 10 m of the water column, is comparable to laboratory studies that have examined the response of phytoplankton to increased mixing (e.g. Peters and Gross, 1994; Romero et al., 2012). The PSD for this diatom-dominated environment does indicate that a change in size has occurred, though supporting evidence

in the literature is scarce. In a recent investigation into the size structure of phytoplankton communities exposed to varying levels of turbulence, Cozar and Echevarria (2005) demonstrated that colonies of the chain-forming *Skeletonema costatum* do undergo breakage when turbulence is enhanced to levels matching that seen in the upper water column. It is this species of diatom that dominates the phytoplankton biomass at L4 within the size range that the holocam is able to resolve (Widdicombe et al., 2010). Lab-based experiments do not tend to report the destruction of phytoplankton chains when the level of turbulent dissipation is of the order of $10^{-6}\,\mathrm{W\,kg^{-1}}$ (Peters et al., 2002; Arin et al., 2002), which is the highest value observed below 10 m at the 16:00 time point.

There remains some difficulty in translating studies in the lab to the field, particularly with respect to phytoplankton and turbulence (Thornton, 2002). Rarely do two different mechanisms for generating mechanically-induced turbulence conform to the same standard, and rarer still are the studies that induce comparable turbulent intensities (Drapeau et al., 1994). Methods for conducting experiments in the lab with phytoplankton and turbulence have changed little over the previous 20 years, and it is unclear how well these studies approximate field conditions. In light of this, the results presented here suggest that moderate levels of turbulence are perhaps capable of impacting on the size of diatom chains, though clearly further work will be needed to confirm if this is accurate.

The reduction in number of phytoplankton is also a function of how they are classified throughout this work. The increased frequency with which diatoms collide with other particles and form flocs has contributed to this decline, and according to our scheme would no longer be considered phytoplankton particles having done so. Diatoms will readily aggregate, typically in response to increased mixing where contact with other material in the water column can habitually occur (Kranck and Milligan, 1988; Kiorboe et al., 1994; Burd and Jackson, 2009). The images from the latter part of

the survey support this, indicating that there is a balance between particle break-up which is reducing size, and an enhanced rate of collision which is contributing to a change in particle composition. Such detail on the fate of phytoplankton subjected to turbulence has not been previously observed *in situ*. That this is also occurring at relatively moderate levels of turbulence is perhaps surprising, suggesting there is a need for greater effort to reconcile laboratory experiments with field data. Further work utilising the relatively new method of holographic imaging will undoubtedly help in this, as the need for reliable information on the impact of short-term mixing events on phytoplankton communities becomes increasingly important for accurate numerical simulations and ecosystem modeling.

5. Acknowledgements

This work was supported by a NERC-funded grant NE/G52388X/1, and also by EU MyOcean (218812) R&D PB-LC 10-103. Many thanks to the crew of the *RV Quest*, and to Emlyn Davies and Fred Wobus for additional labour. We would also like to extend our thanks to the two anonymous reviewers whose comments help to improve this paper.

References

Arin, L., Marrase, C., Maar, M., Peters, F., Sala, M., Alcaraz, M., 2002. Combined effects of nutrients and small-scale turbulence in a microcosm experiment. i dynamics and size distribution of osmotrophic plankton. Aquatic Microbial Ecology 29, 51–61.

Burd, A.B., Jackson, G.A., 2009. Particle Aggregation. Annual Review of Marine Science 1, 65–90.

Cozar, A., Echevarria, F., 2005. Size structure of the planktonic community in microcosms with different levels of turbulence. Scientia Marina 69, 187–197.

454 Cross, J., Nimmo Smith, W.A.M., Torres, R., Hosegood, P., 2013. Biological
455 controls on resuspension and the relationship between particle size and
456 the Kolmogorov length scale in a shallow coastal sea. Marine Geology 343,
457 29–38.

458 Drapeau, D., Dam, H., Grenier, G., 1994. An improved flocculator design for
459 use in particle aggregation experiments. Limonology and Oceanography
460 39, 723–729.

461 Fishwick, J., 2008. Biological and photo-physiological interactions between
462 phytoplankton functional types; a five year study in the western English
463 Channel. Ph.D. thesis. University of Plymouth.

464 Gallienne, C., Robins, D., 2001. Is oithona the most important copepod in
465 the worlds oceans? Journal of Plankton Research 23, 1421–1432.

466 Graham, G., Davies, E., Nimmo-Smith, W., Bowers, D., Braithwaite, K.,
467 2012. Interpreting lisst-100x measurements of particles with complex shape
468 using digital in-line holography. Journal of Geophysical Research 117,
469 C05034.

470 Graham, G., Nimmo Smith, W.A.M., 2010. The application of holography to
471 the analysis of size and settling velocity of suspended cohesive sediments.
472 Limnology and Oceanography - Methods 8, 1–15.

473 Groom, S., Martinez-Vicente, V., Fishwick, J., Tilstone, G., Moore, G.,
474 Smyth, T., Harbour, D., 2009. The Western English Channel observa-
475 tory: Optical characteristics of station L4. Journal of Marine Systems
476 77, 278–295. Workshop on Coastal Observatories - Best Practice in the
477 Synthesis of Long-Term Observations and Models, Liverpool, ENGLAND,
478 OCT 16-19, 2006.

479 Hill, P., 1998. Controls on floc size in the sea. Oceanography 11, 13–18.

480 Jago, C.F., Jones, S.E., Sykes, P., Rippeth, T., 2006. Temporal variation of
481 suspended particulate matter and turbulence in a high energy, tide-stirred,
482 coastal sea: Relative contributions of resuspension and disaggregation.
483 Continental Shelf Research 26, 2019–2028.

484 Jumars, P.A., Trowbridge, J.H., Boss, E., Karp-Boss, L., 2009. Turbulence-
485 plankton interactions: a new cartoon. Marine Ecology - An Evolutionary
486 Perspective 30, 133–150.

487 Kiorboe, T., Lundsgaard, C., Olesen, M., Hansen, J., 1994. Aggregation and
488 sedimentation processes during a spring phytoplankton bloom : a field
489 experiment to test coagulation theory. Journal of Marine Research 52,
490 297–323.

491 Kranck, K., Milligan, T., 1988. Macroflocs from diatoms - in situ photog-
492 raphy of particles in bedford basin, nova-scotia. Marine Ecology Progress
493 Series 44, 183–189.

494 Lozovatsky, I., Roget, E., Fernando, H., Figueroa, M., Shapovalov, S., 2006.
495 Sheared turbulence in a weakly stratified upper ocean. Deep Sea Research
496 Part I: Oceanographic Research Papers 53, 387–407.

497 Macias, D., Rodriguez-Santana, A., Ramirez-Romeo, E., Bruno, M., Pelegri,
498 J., Sangra, P., Aguiar-Gonzalez, B., Garcia, C., 2013. Turbulence as a
499 driver for vertical plankton distribution in the subsurface upper ocean.
500 Scientia Marina 77, 541–549.

501 Manning, A., Dyer, K., 1999. A laboratory examination of floc characteristics
502 with regard to turbulent shearing. Marine Geology 160, 147–170.

503 Mitchell, J., Yamazaki, H., Seuront, L., Wolk, F., Li, H., 2008. Phytoplank-
504 ton patch patterns: Seascape anatomy in a turbulent ocean. Journal of
505 Marine Systems 69, 247–253.

Peters, F., Gross, T., 1994. Increased grazing rates of micro-plankton in response to small-scale turbulence. Marine Ecology Progess Series 115, 299–307.

Peters, F., Marrase, C., Havskum, H., Rassoulzadegan, F., Dolan, J., Alcaraz, M andGasol, J., 2002. Turbulence and the microbial food web: effects on bacterial losses to predation and on community structure. Journal of Plank 24, 321–331.

Prairie, J., Franks, P., Jaffe, J., Doubell, M., Yamazaki, H., 2011. Physical and biological controls of vertical gradients in phytoplankton. Limnology and Oceanography: Fluids & Environments 1, 75–90.

Prandke, H., 2005. Microstructure Sensors. Cambridge University Press. chapter in: Marine Turbulence: theories, observations, and models. Results of the Cartum Project. pp. 101–109.

Rippeth, T., Inall, M., 2002. Observations of the internal tide and associated mixing across the Malin Shelf. Journal of Geophysical Research - Oceans 107.

Romero, E., Peters, F., Marrase, C., 2012. Dynamic forcing of coastal plankton by nutrient imbalances and match-mismatch between nutrients and turbulence. Marine Ecology Progess Series 464, 69–87.

Rzadkowolski, C., Thornton, D., 2012. Using laser scattering to identify diatoms and conduct aggregation experiments. European Journal of Phycology 47, 30–41.

Sharples, J., 2008. Potential impacts of the spring-neap tidal cycle on shelf sea primary production. Journal of Plankton Research 30, 183–197.

Sharples, J., Moore, C., Rippeth, T., Holligan, P., Hydes, D., Fisher, N., Simpson, J., 2001. Phytoplankton distribution and survival in the thermocline. Limonology and Oceanography 46, 486–496.

Simpson, J., Crawford, W., Rippeth, T., Campbell, A., Cheok, J., 1996. The vertical structure of turbulent dissipation in shelf seas. Journal of Physical Oceanography 26, 1579–1590.

Simpson, J.H., Brown, J., Matthews, J., Allen, G., 1990. Tidal straining, density currents and stirring in the control of estuarine stratification. Estuaries 13, 125–132.

Smyth, T.J., Fishwick, J.R., Al-Moosawi, L., Cummings, D.G., Harris, C., Kitidis, V., Rees, A., Martinez-Vicente, V., Woodward, E.M.S., 2010. A broad spatio-temporal view of the Western English Channel observatory. Journal of Plankton Research 32, 585–601.

Steinbuck, J.V., Stacey, M.T., McManus, M.A., Cheriton, O.M., Ryan, J.P., 2009. Observations of turbulent mixing in a phytoplankton thin layer: Implications for formation, maintenance, and breakdown. Limnology and Oceanography 54, 1353–1368.

Stemmann, L., Boss, E., 2012. Plankton and particle size and packaging: From determining optical properties to driving the biological pump. Annual Reviee of Marine Science 4, 263–290.

Sutherland, G., Ward, B., Christensen, K., 2013. Wave-turbulence scaling in the ocean mixed layer. Ocean Science 9, 597–608.

Thornton, D., 2002. Diatom aggregation in the sea : mechanisms and ecological implications. European Journal of Phycology 37, 149–161.

Widdicombe, C.E., Eloire, D., Harbour, D., Harris, R.P., Somerfield, P.J., 2010. Long-term phytoplankton community dynamics in the western English Channel. Journal of Plankton Research 32, 643–655.

Zarauz, L., Irigoien, X., Fernandes, J.A., 2009. Changes in plankton size structure and composition, during the generation of a phytoplankton

559 bloom, in the central cantabrian sea. Journal of Plankton Research 31,
560 193–207.